

**Original citation:**

De Giovanni, Mario, Warnett, Jason M., Williams, Mark A. and Srirangam, Prakash. (2017) 3D imaging and quantification of porosity and intermetallic particles in strontium modified Al-Si alloys. Journal of Alloys and Compounds .

**Permanent WRAP URL:**

<http://wrap.warwick.ac.uk/91715>

**Copyright and reuse:**

The Warwick Research Archive Portal (WRAP) makes this work by researchers of the University of Warwick available open access under the following conditions. Copyright © and all moral rights to the version of the paper presented here belong to the individual author(s) and/or other copyright owners. To the extent reasonable and practicable the material made available in WRAP has been checked for eligibility before being made available.

Copies of full items can be used for personal research or study, educational, or not-for-profit purposes without prior permission or charge. Provided that the authors, title and full bibliographic details are credited, a hyperlink and/or URL is given for the original metadata page and the content is not changed in any way.

**Publisher's statement:**

© 2017, Elsevier. Licensed under the Creative Commons Attribution-NonCommercial-NoDerivatives 4.0 International <http://creativecommons.org/licenses/by-nc-nd/4.0/>

**A note on versions:**

The version presented here may differ from the published version or, version of record, if you wish to cite this item you are advised to consult the publisher's version. Please see the 'permanent WRAP url' above for details on accessing the published version and note that access may require a subscription.

For more information, please contact the WRAP Team at: [wrap@warwick.ac.uk](mailto:wrap@warwick.ac.uk)

# 3D imaging and quantification of porosity and intermetallic particles in strontium modified Al-Si alloys

Mario De Giovanni<sup>1</sup>, Jason M. Warnett<sup>1</sup>, Mark A. Williams<sup>1</sup>, Prakash Srirangam<sup>1\*</sup>

<sup>1</sup> Warwick Manufacturing Group (WMG), University of Warwick, Coventry, CV4 7AL, UK

\* Corresponding author: *Prakash Srirangam* (p.srirangam@warwick.ac.uk)

Tel: +044-2476573662

## Abstract

Al-Si alloys are widely used in the automotive and aerospace industries. Porosity is considered to be a major defect in these cast alloys. In this study, the effect of strontium (Sr) modification on porosity formation and intermetallic formation in Al-Si alloys is quantified using X-ray tomography. Quantitative information such as average pore size, shape, pore distribution and intermetallic particle size distribution were evaluated for Sr modified and unmodified Al-Si alloys. Results show that the addition of 400 ppm of Sr increases the porosity by 10% as compared to unmodified Al-Si alloy. Further, Sr addition increases the average equivalent diameter of pores from 2  $\mu\text{m}$  to 18  $\mu\text{m}$  compared to unmodified alloys. A greater number of larger pores were found in the Sr modified alloy, whereas the number of small sized pores was significantly higher in unmodified alloy. The addition of 400 ppm of Sr results in formation of Al-Si-Sr intermetallics with an average equivalent diameter of 4.5  $\mu\text{m}$ . It can be hypothesised that these intermetallic particles act as heterogeneous sites for pore nucleation and significant further growth of porosity in Sr modified alloys.

**Keywords:** Al-Si alloys, Sr modification, micro porosity,  $\text{Al}_2\text{Si}_2\text{Sr}$  intermetallics, X-ray tomography.

## 1. Introduction

Aluminium-Silicon (Al-Si) alloys are widely used in the automotive, aerospace and casting industries due to their excellent strength to weight ratio, high corrosion resistance, good weldability, excellent mechanical and performance properties [1]. Eutectic silicon appears in the form of needles or platelets which results in poor mechanical properties of these alloys. To reduce this effect, these alloys are usually treated with trace level additions of modifying elements such as sodium or strontium and rare earth elements etc. [1,2]. Strontium is typically used due to its high retention and low over-modification issues in cast Al-Si alloys. Although strontium modification improves microstructure and mechanical properties [1–3], it also results in a significant increase in porosity that negatively impacts the fatigue properties of cast alloy [4–8].

Porosity in Al-Si cast alloys occurs as gas porosity or shrinkage porosity [9]. Emadi et al [9] list several factors that could lead to an increase in porosity due to strontium modification in Al-Si alloys; an increase in hydrogen content of melt, an absorption of hydrogen to oxides, a decrease in solubility of hydrogen during solidification, a depression in eutectic temperature, an increase in inclusion content, a decrease in surface tension of molten metal and an increased volumetric shrinkage of the alloy. Emadi et al [9] noted that addition of 0.01 wt% Sr to A356 alloy decreases the surface tension by 19% and increases the volumetric shrinkage by 12%. Furthermore, it was observed that the modification treatment promotes the early formation of pores during solidification thus allowing more time for large pores to develop [9,10]. Several studies suggested that in unmodified alloys the eutectic liquid seemed to flow between interdendritic regions, while, Sr modification affects the bifilms' retention in liquid which restricts the mobility of liquid into interdendritic regions thereby increasing porosity content in the alloys [11–13]. A number of studies have shown that the presence of oxides increases porosity by decreasing the fluidity of the melt [14–18].

Though much research has been carried out to understand the porosity formation in Sr modified alloys, the mechanism is still unclear. Understanding porosity formation and its increase in Sr modified Al-Si alloys is essential to improve the melt quality, mechanical properties and to reduce hot tearing and wastage of castings. This porosity is one of the main reasons for fatigue cracks initiation in the castings [19–22]. Researchers have observed a direct correlation between pore size and shape to resultant fatigue life of cast components [19,23]. Most of these studies were carried out using conventional microscopy techniques which provides 2D microstructural images of pores, used to predict the mechanical properties of Al-Si alloys. Since pores will have different shapes and morphologies in different orientations, it is essential to visualise and quantify them in 3D to better predict the mechanical properties of these alloys.

X-ray Computed Tomography (XCT) is a powerful non-destructive technique which provides a three-dimensional (3D) visualisation of internal structure inhomogeneities representative of bulk sample [24–26]. XCT has been applied in numerous fields of research such as medical [27], geology [28] and civil engineering [29]. Several XCT studies were carried out in the past on characterising porosity in Al alloys using XCT and using this data in predicting fatigue properties of these alloys. However, the resolutions obtained in these studies varied between 1.7 – 30  $\mu\text{m}$  [30–34]. In this study, for the first time, lab-based submicron resolution XCT was used to visualise and quantify porosity in Sr modified Al-Si alloys and compare to an unmodified alloy. Furthermore, the formation of Al-Si-Sr intermetallics in Sr modified Al-Si alloys were studied using XCT and SEM analysis.



## 2. Experimental Methods

### 2.1 Alloy preparation

Al-7Si (wt%) alloy was prepared by melting 99.999% purity aluminium (NewMet, UK) in a clay graphite crucible using a Carbolite RHF1500 high temperature chamber furnace. High purity (99.999%) silicon (Alfa Aesar, UK) was added to the molten aluminium and stirred to ensure mixing of silicon in the melt. Once the silicon dissolved in the melt, the mixture was poured into a graphite cylindrical mould (12 mm diameter, 85 mm deep). A portion of the Al-7Si alloy was then used to prepare modified Al-7Si-0.04Sr (wt%) alloy. When the Al-7Si alloy was in a molten state, the Al-10Sr (wt%) master alloy was added to the melt, and returned to the same mould. The cooling rate was approximately 75 °C/s. For XCT measurements, samples with a diameter of 1 mm were machined from the centre of the cast using wire EDM.

### 2.2 X-ray computed tomography

XCT measurements were performed using the Zeiss Versa 520 system. The cylindrical samples with 1 mm diameter were mounted on the rotating stage in the XCT machine. As X-rays pass through the sample, they are either attenuated or pass through the sample resulting in a grey-scale radiograph on the detector screen. Numerous radiographic projections obtained through a 360 degree rotation were then reconstructed into a 3D volume through the process of filtered back projection. The volume consisted of a number of 3D pixels called voxels with an associated grey value between 0 and 65535, proportional to the attenuation of the material.

**Table 1:** X-ray tomography scanning parameters

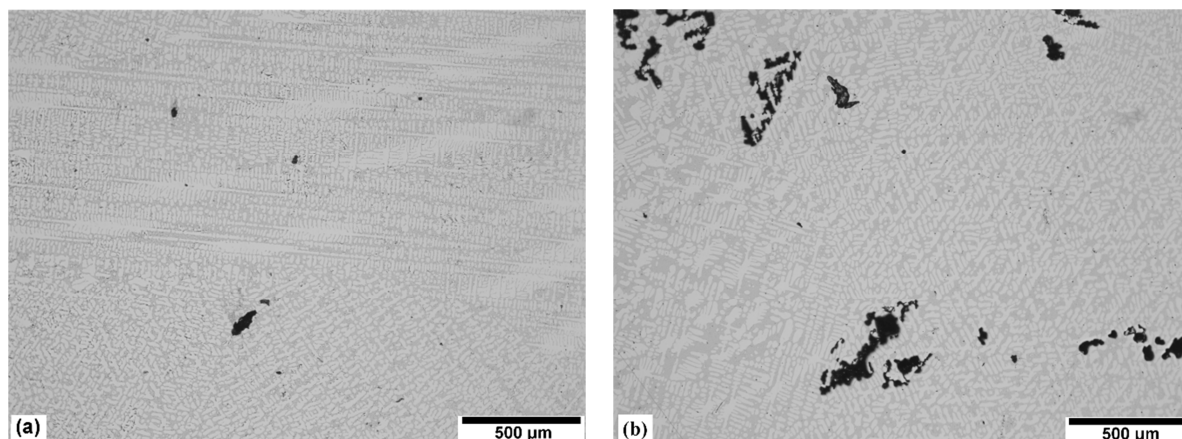
Voltage (kV)	80
Power (W)	7
Exposure (s)	24
Filter (SiO <sub>2</sub> , mm)	0.35
Number of Projections	3201
Voxel size (nm)	390

The XCT scan parameters are given in table 1. In the scans provided for this study a 20x optic was used in combination with a 2000 \* 2000 pixel detector. This resulted in a 390 nm voxel size in the reconstructed volume, measuring 780 \* 780 \* 780 microns. The imaged volumes were segmented using a watershed based algorithm in Avizo 9.3 (FEI, USA) [35]. The principles of image segmentation and XCT operation can be found in an earlier publication [36].

### 2.3 Cooling curves

The progression of solidification of the two samples was analysed by examining their respective cooling curves. Approximately 15 g of each sample were placed in a clay graphite crucible and melted at 750 °C in an electrical resistance furnace. Once molten, the crucible was taken out and immediately a K-type thermocouple was inserted below the surface of the melt. The cooling curve was collected using a data logger recording at 10 Hz. A cooling rate of 1.2 °C/s was observed.

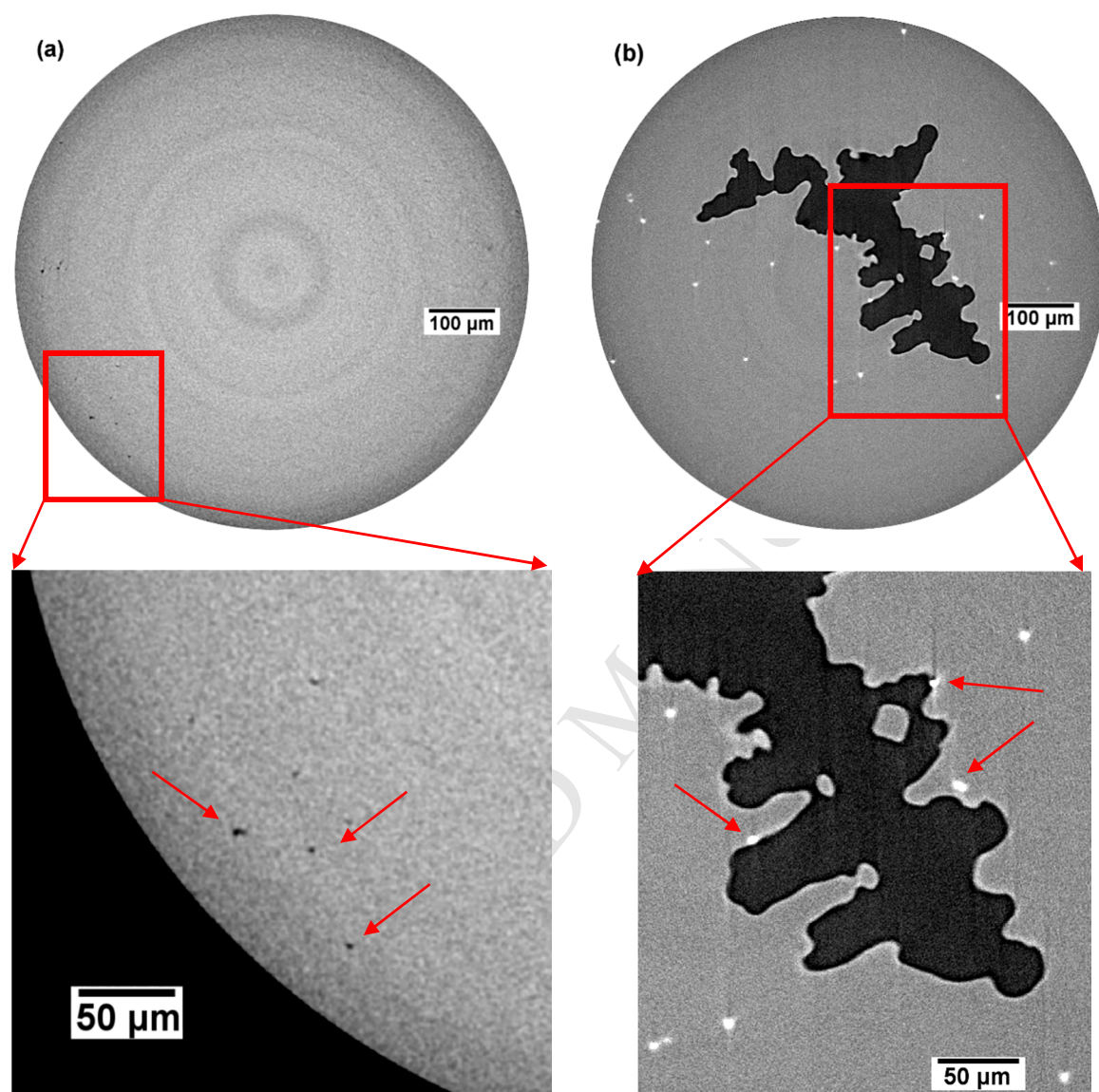
### 3. Results and Discussion



**Figure 1:** Optical microscopy images of (a) Al-7Si, and (b) Al-7Si-0.04Sr.

Figure 1 shows the optical microscopy images of Al-7Si and Al-7Si-0.04Sr modified alloys. It is clearly evident from figure 1 that there is a significant difference in the porosity distribution in the two alloys. The unmodified alloy shows less porosity with a few small pores as represented in figure 1 (a), while, the modified alloy shows higher porosity with the presence of large pores shown in figure 1 (b). Figure 2 (a and b) shows XY ortho slices in Al-7Si and Al-7Si-0.04Sr alloy samples respectively from XCT measurements. It is evident that the Al-7Si unmodified alloy contains very fine pores (fig 2a), whereas the Al-7Si-0.04Sr modified alloy contains extremely large pores (fig 2b). The insets in these images represent higher magnification images showing different pore features in the two alloys. As shown in figure 2 (a), an area is magnified for highlighting small pores in the unmodified alloy. In the modified alloy, the magnified image figure 2 (b) clearly shows the presence of intermetallic particles represented by bright spots. The scanned samples were taken from the centre of the alloy castings where it is known that porosity is higher [37]. Figure 2 (c and d) represents the complete three-dimensional reconstructions of porosity and intermetallic particles in unmodified and Sr modified Al-Si alloys respectively. The green, blue and red colours in

figure 2 (c and d) represents the Al matrix, porosity and intermetallic particles in cast alloys respectively.



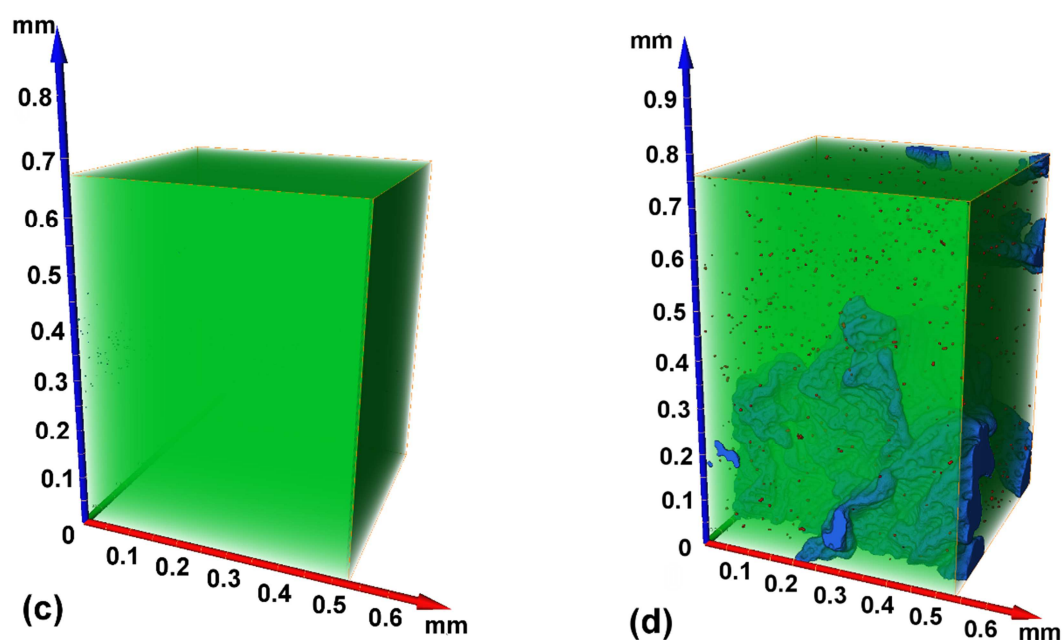


**Figure 2:** XY ortho slices in (a) Al-7Si showing the presence of small pores and (b) Al-7Si-0.04Sr showing the presence of a large pore and smaller intermetallic particles. The insets show higher magnification images. In the Al-7Si inset, the small pores can be observed better, whereas in the Al-7Si-0.04Sr the intermetallics surrounding the pore are highlighted. Full 3D reconstructed images of (c) Al-7Si alloy showing the matrix (green) and pores (blue) and (d) Al-7Si-0.04Sr alloy showing the matrix (green), pores (blue) and particles (red).

In figure 3 the matrix is removed from view displaying only the pores. Since the pores are particularly small in the Al-Si alloy, they have been dilated 3x for visualisation purposes. The unmodified Al-Si alloy contains a large number of small pores (figure 3a) which are mainly located in the central region of the sample, compared to the significantly larger pores observed with the addition of Sr (figure 3b). There are still a limited number of smaller pores in the Al-Si-Sr alloy, but the large pores dominate the image. In order to visualise the smaller pores, the larger pores have been removed and the smaller pores dilated by 3x in figure 3 (c). Furthermore it can be noted that in figure 3 (b) the pores are in contact with the edge of the boundary box. This suggests that these pores extend beyond the boundary box and thus it is likely that the sizes of these pores is underestimated.



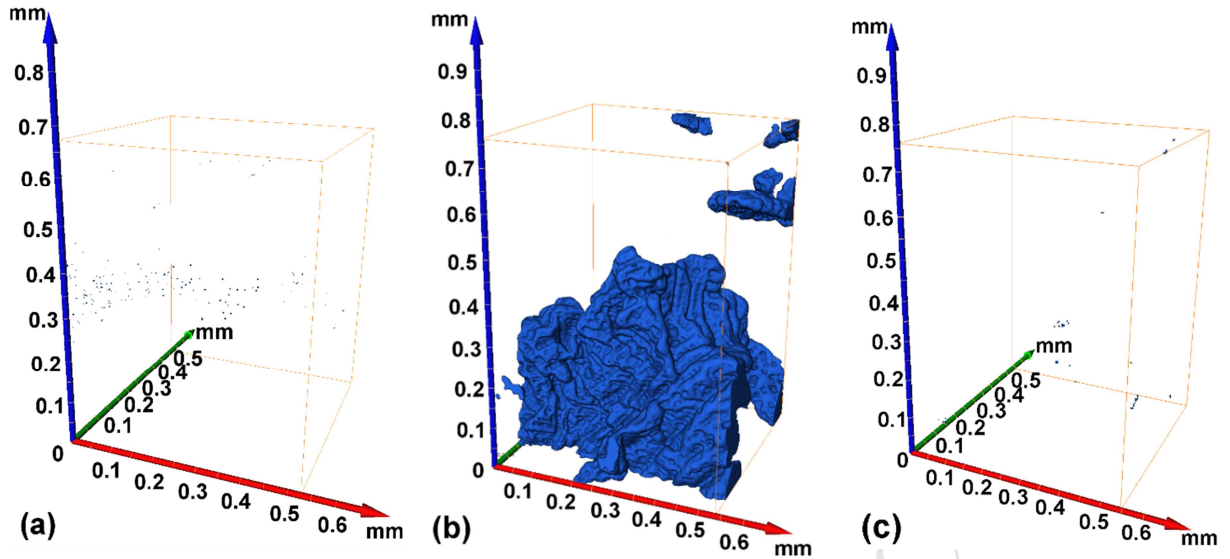


**Figure 3:** 3D reconstruction of pores from XCT data in (a) Al-7Si, (b) Al-7Si-0.04Sr and (c) Al-7Si-0.04Sr following the removal of large pores. For visualisation purposes the pores in (a) and (c) were dilated by 3x.

To assess the porosity shape and size distribution in unmodified and modified alloys, XCT data was analysed using Avizo and is presented in figure 4. Figure 4 (a) shows that the vast majority of the pores in the Al-7Si alloy were found to have an equivalent diameter which is less than 2  $\mu\text{m}$ , with the largest pore having an equivalent diameter which is approximately 4  $\mu\text{m}$ . In order to understand the shape change of pores due to Sr addition, sphericity calculations were performed using equation 1. Sphericity is a measure of how spherical a feature is where, a sphericity value of 1 represents a perfect spherical shape of the pore [38].

$$\Psi = \frac{\pi^{\frac{1}{3}}(6V_p)^{\frac{2}{3}}}{A_p} \quad (1)$$

In equation 1,  $\Psi$  represents the sphericity,  $V_p$  represents the volume of a pore,  $A_p$  represents the area of a pore. Figure 4 (b and c) represents the sphericity analysis of Al-7Si. Figure 4 (b) shows that the sphericity value for most of the pores in unmodified alloys is in the range between 0.8 and 0.9 which represents that the pores are close to spherical in shape in unmodified alloy. Figure 4 (c) shows how sphericity varies with the volume of the particle. It

can be noted that almost all pores with an equivalent diameter greater than 2  $\mu\text{m}$  have a sphericity value between 0.7 and 1.0 showing that a pore nucleates in an almost spherical shape. This spherical shape can change as the pore grows further with more diffusion of hydrogen into the nucleated pore during solidification of alloy casting.

Figure 4 (d-f) represents quantification of porosity in the Al-7Si-0.04Sr modified alloy. As shown in figure 4 (d), the modified alloy shows a significant number of large pores with an equivalent diameter  $>5 \mu\text{m}$ . Further it is evident that, the number of small sized pores with an equivalent diameter  $>2 \mu\text{m}$ , were found to be less in number in the modified alloy as compared to the unmodified alloy. The modified alloy shows presence of small pores with an equivalent diameter of 2.5 - 4  $\mu\text{m}$  as well as large pores with an equivalent diameter of 5  $\mu\text{m}$  and above as shown in figure 4 (d). Similar observations were made by Lashkari et al [31] in which they attributed the large size pores formation to hydrogen gas solubility in the alloy and small pores formation to the local entrapment of liquid metal at the end of interdendritic feeding. It is well known that gas pores form in spherical shape but as solidification proceeds, more hydrogen diffuses into already nucleated pores resulting in their growth and ultimately large pore formation in the casting. Figure 4 (e) represents the sphericity of pores in the Al-7Si-0.04Sr modified alloy. The sphericity of pores in the modified alloy is largely confined to values between 0.6 and 0.8, with the exception of a countable few that are very low in sphericity and correlate to the largest pores. Even eliminating these exceptions, the sphericity of the pores in the modified alloy is lower than the Al-7Si cast. This observation is in contradiction to Liao et al's [4] study where they noted that the sphericity in modified alloys is higher compared to unmodified alloys. The presented data is of higher resolution than the previous study, which could account for differences in the perceived sphericity.

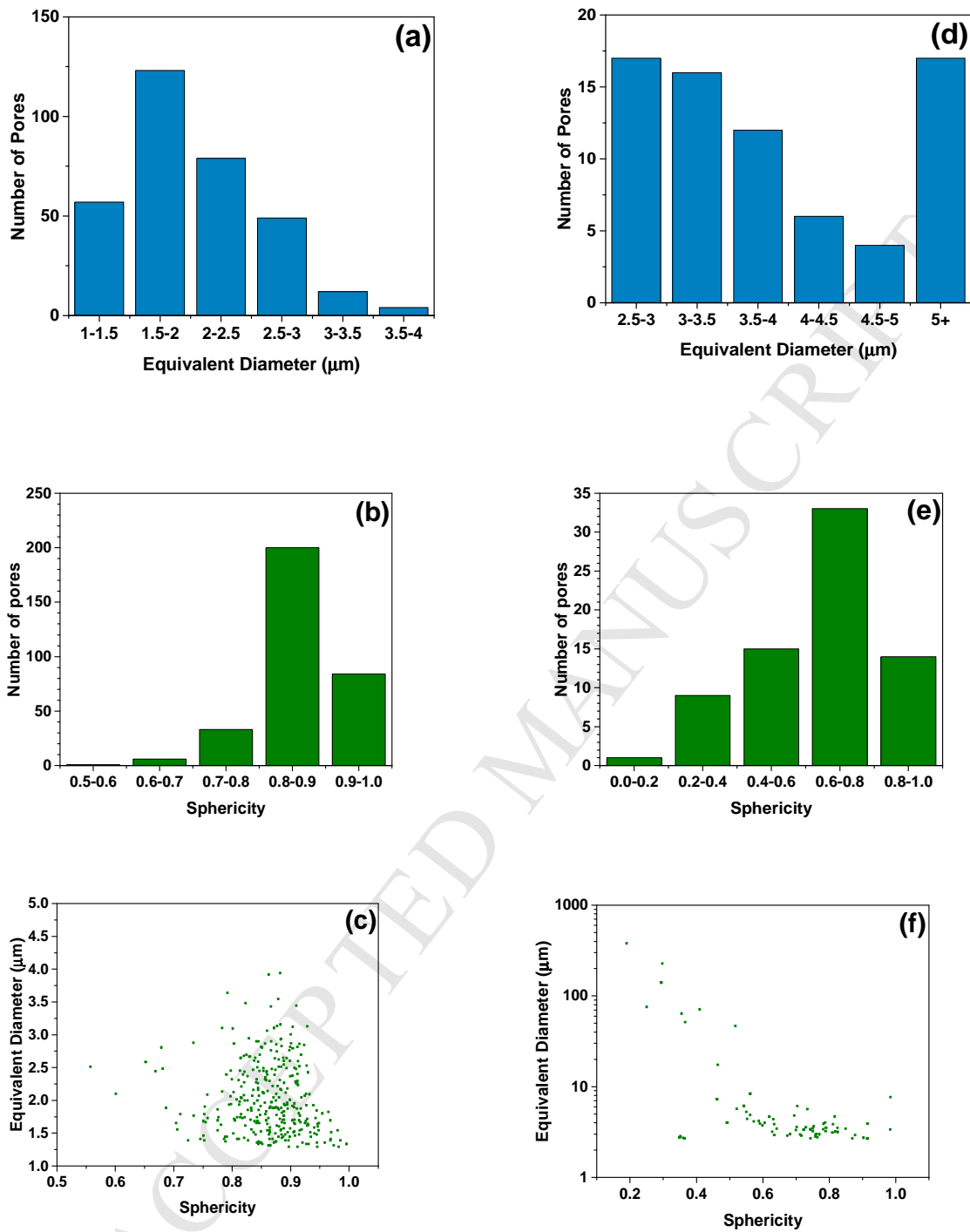


**Figure 4:** Data obtained from XCT for (a-c) Al-7Si, (d-f) Al-7Si-0.04Sr alloy. (a, d) Size distribution of porosity, (b, e) Sphericity of the pores, (c, f) Relationship of sphericity to the size of the pores. Note that the y-scale is different for the two different samples.

Figure 5 (a and b) represents the magnified images of a single largest pore in Al-7Si and Al-7Si-0.04Sr alloys respectively. The largest pore in Al-7Si is close to a spherical shape and is



approximately 0.01 mm in diameter, compared to the Sr modified alloy that is nearly 100 times larger and distinctly non-spherical. This shape of the largest pore in the modified alloy is indicative of shrinkage porosity as it shows the inter-dendritic shape resulting from lack of mass feeding. This kind of dendritic arm impingement on the pore has previously been reported in Al-Si alloys with Si content ( $<10\%$ ) in the alloys [39].

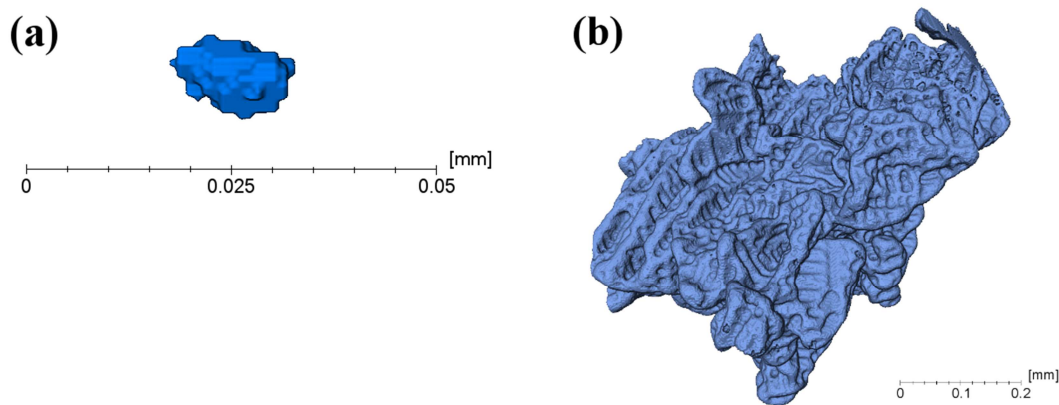


**Figure 5:** 3D reconstructed images of the largest pores in (a) Al-7Si, (b) Al-7Si-0.04Sr.

A numerical comparison of the porosity is given in table 2. It is clear from table 2 that the porosity is only 0.00006% in unmodified alloy, while that in the Sr modified alloy is greater than 10%. Similar observations were made by previous researchers where they noted a reduction in the number of pores but the overall porosity increases due to modification with Sr in Al-Si alloys [4]. This is further shown by comparing the average and maximum pore volumes in the sample, where the maximum pore volume in the Sr modified alloy was found to be six orders of magnitude greater than the unmodified alloy.

**Table 2:** Quantitative information of porosity in Al-7Si and Al-7Si-0.04Sr alloys as well as and intermetallic particles in Al-7Si-0.04Sr.

	Al-7Si	Al-7Si-0.04Sr
Total volume analysed ( $\text{mm}^3$ )	0.290	0.336

Pore percentage (%)	0.00006	11.101
Particle percentage (%)	-	0.034
Average pore equivalent diameter ( $\mu\text{m}$ )	2.03	18.30
Maximum pore equivalent diameter ( $\mu\text{m}$ )	3.94	381.00
Average intermetallic equivalent diameter ( $\mu\text{m}$ )	-	4.52
Maximum intermetallic equivalent diameter ( $\mu\text{m}$ )	-	10.66

Figure 6 shows the presence and quantification of intermetallic particles in the Al-7Si-0.04Sr alloy. The 3D reconstruction of these particles within the alloy is shown in figure 6 (a), where an even spatial distribution is observed. Figure 6 (b) shows the size distribution of these particles where the majority are less than  $6\ \mu\text{m}$ , however a few exceed an equivalent diameter of  $10\ \mu\text{m}$ . Similar to pores, the sphericity of these intermetallic particles was also investigated as shown in figure 6 (c and d). Figure 6 (c) shows that majority of intermetallic particles were close to a value between 0.9 and 1, demonstrating a strongly spherical nature. Furthermore, very few particles (0.3%) have a sphericity value less than 0.8. Figure 6 (d) shows that sphericity values between 0.9 and 1.0 are mainly occupied by particles with an equivalent diameter less than  $6\ \mu\text{m}$ , whilst larger particles tend to be less spherical. Figure 6 (e) shows a magnified image of the largest intermetallic particle in the Sr modified alloy. Miresmaeili et al [40] have observed similar intermetallic particles in A356 alloy modified by 0.04 wt% Sr by SEM, a 2D technique. Sigworth et al [41] note that the usual amount of Sr required for modification is in the range 100-200 ppm and any amount higher than 200 ppm would result in formation of Al-Si-Sr intermetallic compounds. The reason for formation of these particles in the Sr modified alloy in this study is most probably due to higher amounts of Sr in the melt.

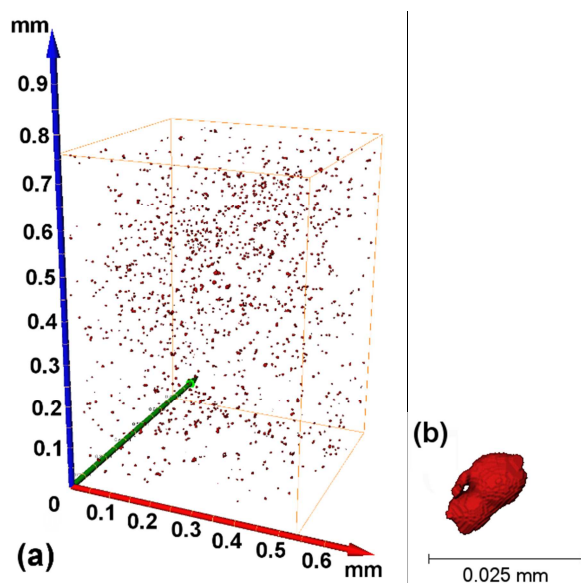


**Figure 6:** XCT and SEM-EDX data for intermetallic particles in Al-7Si-0.04Sr alloy. (a) 3D reconstruction of particles in the alloy, (b) Size distribution of porosity, (c) Sphericity of the pores, (d) Relationship of sphericity to the size of the pores, (e) largest particle in alloy.

In this research, these intermetallic particles were also characterised by means of energy dispersive spectroscopy (EDS). Figure 7 (a) shows a secondary electron image of an intermetallic particle, and its corresponding EDS maps showing presence of Al, Si, Sr and O elements is presented in figure 7 (b-d). When examining the maps the intensity of the colour is representative of the relative intensity of the element. Thus, the black area in the Al map does not mean that there is no Al present but rather that it is much less than in other areas. Furthermore, Si and Sr have overlapping energy lines and thus higher intensity areas of either could simply be wrongly attributed to either element. By using the ‘Trumap’ method in the

Aztec software, a distinction between the two elements could be achieved [42]. Previous research studies indicated that SrO could act as a nucleation site for similar intermetallic particles [40]. The O map shows an area of high O concentration indicating a possibility that this intermetallic particle could have nucleated on a SrO particle. The stoichiometry of these intermetallic particles is difficult to determine from the SEM-EDS, but by inspecting the Al-Si-Sr ternary phase diagram, it can be inferred that these particles are  $\text{Al}_2\text{Si}_2\text{Sr}$  particles [43].

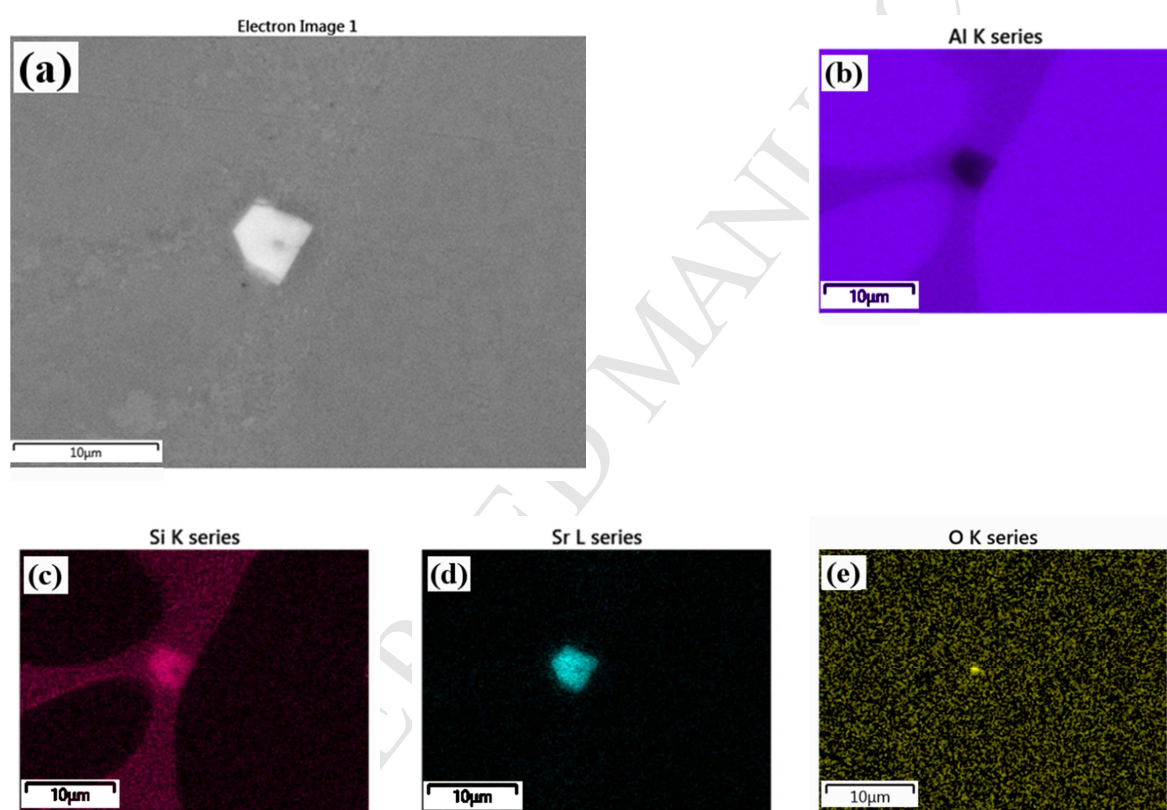


**Figure 7:** SEM-EDS characterisation of intermetallic particle showing (a) SE image, (b) Al EDS map, (c) Si EDS map, (d) Sr EDS map, (e) O EDS map.

Figure 8 (a-d) shows the cooling curves obtained by analysing the unmodified and Sr-modified samples. In this figure the eutectic time growth is indicated along the thermal profiles (a and c), whereas a magnified plot on the eutectic transition (b and d) marks the eutectic nucleation temperature, minimum temperature and growth temperature. The major

differences between the two cooling curves can be identified in the undercooling phase, which is an indication of the microstructural modification, and the eutectic growth time. This longer eutectic time also provides an extended time for porosity growth.

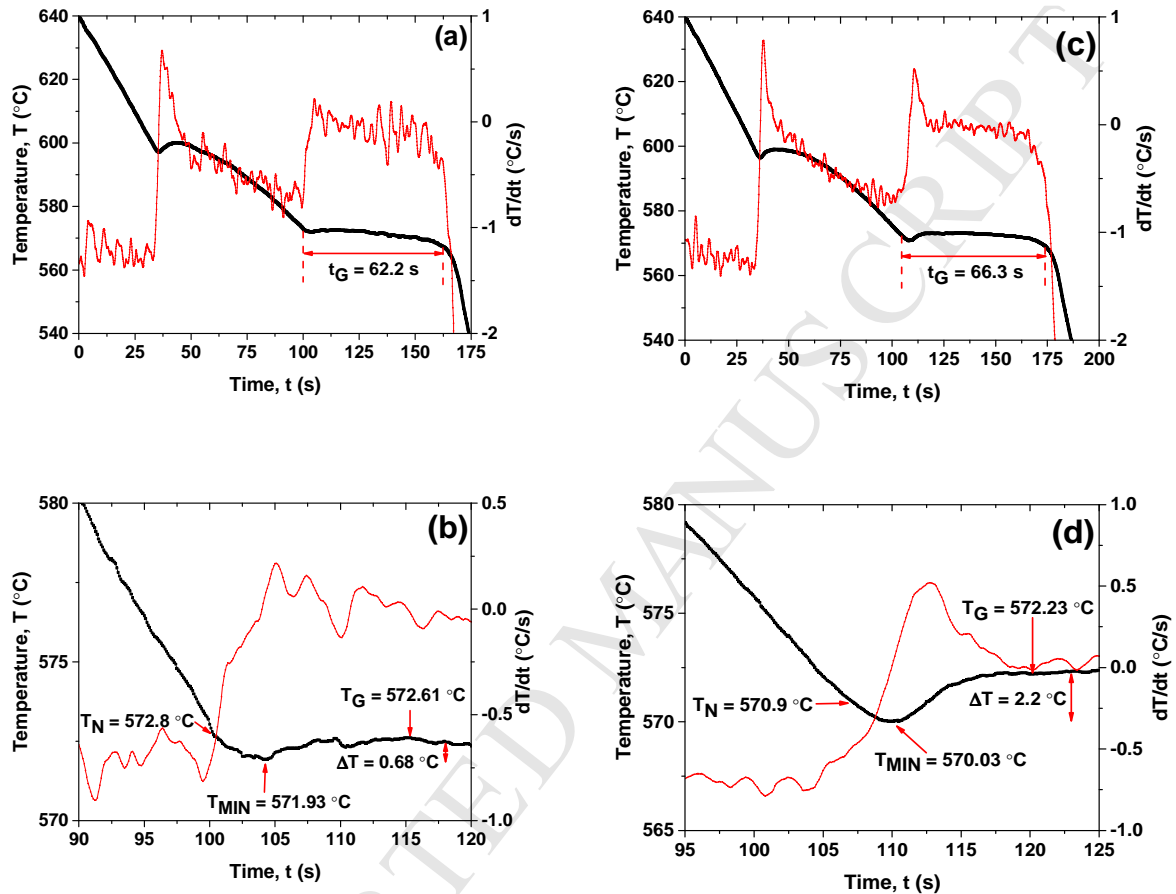


**Figure 8:** Cooling curves showing the (a, c) entire thermal profile and the (b, d) eutectic section for the (a, b) Al-7Si and the (c, d) Al-7Si-0.04Sr. In these images the time of eutectic growth ( $t_G$ ), the eutectic nucleation temperature ( $T_N$ ), minimum temperature ( $T_{MIN}$ ), eutectic growth temperature ( $T_G$ ) and eutectic undercooling ( $\Delta T$ ) are indicated.

This study clearly shows that the XCT is a powerful technique in understanding porosity formation in Al-Si alloys. It is evident that the addition of Sr to Al-Si alloys results in increased porosity compared to unmodified alloys as shown in figure 1 to figure 5 and in table 2. The presence of oxides and intermetallic particles could act as heterogeneous nucleation sites for pore formation and depending on the availability of hydrogen present in

the melt, the pores grow and form large size pores in the castings. Denton et al [37] observed that the melt hydrogen content increases upon addition of 0.04% Sr in Al-Si alloys. Samuel et al [44] observed that the presence of impurities, such as Al-Sr-O or Al-Si-Sr, close to pores and hypothesised that these particles act as heterogeneous nucleation sites for porosity formation, with similar observations found in this study shown in figure 2 (b). Further, from differential analysis and cooling curve studies in figure 8 it is evident that the undercooling of the melt and eutectic solidification time increased upon addition of Sr to alloy. This increase in solidification time increases the freezing range and length of the mushy zone which ultimately results in an increase in porosity formation in modified alloys. With an increase in solidification time, there is more time for nucleated pore to grow with more hydrogen to diffuse into it. Atwood et al [5] developed a model for pore nucleation rate as a function of time and found that the increase in undercooling increases the pore nucleation sites. Once the pore nucleated, hydrogen diffuses into them resulting in pore growth and large pore formation. Figure 5 clearly shows that the pores in Sr modified alloys are significantly larger in size compared to pores observed in unmodified alloy. Felberbaum et al [45] studied pore morphology in Al-Cu alloys using XCT and found in their 3D rendering that interdendritic porosity originates from bifilms present in the alloy. Campbell [46] noted that pores can nucleate either from particles or bifilms present in the alloy. In this study, for the first time we have shown that the presence of intermetallic particles could act as nucleating sites for pores in Sr modified Al-Si alloys. It is difficult to confirm whether pores nucleated on these intermetallic particles as samples were studied on solidified alloys. Future studies involving in-situ synchrotron 3D XCT studies during solidification from molten state would further aid in understanding the mechanism of pore nucleation and pore growth in aluminium alloy castings.

#### 4. Conclusions

- X-ray tomography was used to quantify porosity and intermetallic particles in Sr modified Al-Si alloys. The visualisation of pores and intermetallic particles in these alloys was carried out using a high resolution XCT with a voxel size of 390 nm.
- XCT results show that the addition of 400 ppm of Sr to Al-Si alloy resulted in a higher volume fraction of porosity (by over 10%) compared to unmodified alloys. Further it was observed that the average equivalent diameter of pore increased from 2  $\mu\text{m}$  to 18  $\mu\text{m}$  upon addition of Sr.
- The XCT analysis of Sr modified alloy allowed for the analysis of the intermetallic particles present in the Sr-modified alloy. These intermetallic particles occupy a volume fraction of 0.03% and have an average equivalent diameter of 4.5  $\mu\text{m}$ . SEM-EDS analysis confirms the presence and formation of  $\text{Al}_2\text{Si}_2\text{Sr}$  type intermetallic compounds in Sr modified Al-Si alloys.
- This study shows that the Sr modification results in formation of intermetallic particles and the presence of these intermetallic particles could act as heterogeneous sites for pore nucleation in the alloys. Further, it was shown that Sr modification affects undercooling and eutectic temperature which allows more time for already nucleated pore to grow into a large size pore in modified alloys compared to unmodified alloys.

#### References

- [1] I.J. Polmear, Cast Aluminium Alloys, in: Light Alloy., Elsevier, 2005: pp. 205–235. doi:10.1016/B978-075066371-7/50008-6.
- [2] R. Bartley, British and European Aluminium Casting Alloys, Association of Light Alloy Refiners, Birmingham, 1996.



- [3] J.E. Hatch, *Aluminium: Properties and Physical Metallurgy*, 2nd ed., American Society of Metals, 1984.
- [4] H.C. Liao, W. Song, Q.G. Wang, L. Zhao, R. Fan, F. Jia, Effect of Sr addition on porosity formation in directionally solidified A356 alloy, *Int. J. Cast Met. Res.* 26 (2013) 201–208. doi:10.1179/1743133613Y.0000000053.
- [5] R.C. Atwood, S. Sridhar, P.D. Lee, Equations for nucleation of hydrogen gas pores during solidification of aluminium seven weight percent silicon alloy, *Scr. Mater.* 41 (1999) 1255–1259. doi:10.1016/S1359-6462(99)00297-3.
- [6] G.E. Byczynski, D.A. Cusinato, The effects of strontium and grain refiner additions on the fatigue and tensile properties of industrial Al-Si-Cu-Mg alloy castings produced using the Ford Motor Company - Cosworth precision sand process, *Int. J. Cast Met. Res.* 15 (2002) 315–324.
- [7] A. Hetke, R.B. Grundlach, Aluminum casting quality in alloy 356 engine components, *AFS Trans.* 102 (1994) 367–380.
- [8] M. Brosnan, S. Shivkumar, Elevated Temperature Tensile Properties and Fracture Behavior of A356 Castings, *AFS Trans.* 103 (1995) 727–737.
- [9] D. Emadi, J.E. Gruzleski, J.M. Toguri, The effect of Na and Sr modification on surface tension and volumetric shrinkage of A356 alloy and their influence on porosity formation, *Metall. Trans. B.* 24 (1993) 1055–1063. doi:10.1007/BF02660997.
- [10] J. Campbell, M. Tiryakioğlu, Review of effect of P and Sr on modification and porosity development in Al–Si alloys, *Mater. Sci. Technol.* 26 (2010) 262–268. doi:10.1179/174328409X425227.
- [11] R. Fuoco, E.R. Correa, A.V.O. Correa, Effect of modification treatment on



- microporosity formation in 356 Al alloy, AFS Trans. 103 (1995) 379–387.
- [12] R. Fuoco, E.R. Correa, H. Goldenstein, The effect of modification treatment on microporosity formation in 356 Al Alloy, part I: Interdendritic Feeding Evaluation, AFS Trans. 104 (1996) 1151–1158.
- [13] R. Fuoco, E.R. Correa, M. de A. Bastos, Effects of Grain Refinement on Feeding mechanisms in A356 Aluminum Alloy, AFS Trans. 106 (1998) 401–409.
- [14] D.E. Groteke, Influence of SNIF Treatment on Characteristics of Aluminium Foundry Alloys, AFS Trans. 93 (1985) 953–960.
- [15] M. Di Sabatino, S. Rørvik, A. Prestmo, The influence of oxide inclusions on the fluidity of Al–7wt.%Si alloy, Mater. Sci. Eng. A. 413 (2005) 272–276.  
doi:10.1016/j.msea.2005.08.175.
- [16] L. Liu, M. Samuel, F.H. Samuel, H.W. Doty, S. Valtierra, The role of Sr oxide on porosity, AFS Trans. 110 (2002) 449–462.
- [17] H. Iwahori, K. Yonekura, Y. Yamamoto, M. Nakamura, Occurring Behavior of Porosity and Feeding Capability of Sodium- and Strontium- Modified Al-Si Alloys, AFS Trans. 98 (1990) 167–173.
- [18] L. Liu, A.M. Samuel, F.H. Samuel, H.W. Doty, S. Valtierra, Influence of oxides on porosity formation in Sr-treated Al-Si casting alloys, J. Mater. Sci. 38 (2003) 1255–1267. doi:10.1023/A:1022870006721.
- [19] J.Z. Yi, Y.X. Gao, P.D. Lee, H.M. Flower, T.C. Lindley, Scatter in fatigue life due to effects of porosity in cast A356-T6 aluminum-silicon alloys, Metall. Mater. Trans. A. 34 (2003) 1879–1890. doi:10.1007/s11661-003-0153-6.
- [20] J.Z. Yi, P.D. Lee, T.C. Lindley, T. Fukui, Statistical modeling of microstructure and

- defect population effects on the fatigue performance of cast A356-T6 automotive components, *Mater. Sci. Eng. A.* 432 (2006) 59–68. doi:10.1016/j.msea.2006.07.003.
- [21] D.-F. Mo, G.-Q. He, Z.-F. Hu, X.-S. Liu, W.-H. Zhang, Effect of microstructural features on fatigue behavior in A319-T6 aluminum alloy, *Mater. Sci. Eng. A.* 527 (2010) 3420–3426. doi:10.1016/j.msea.2010.02.055.
- [22] Q.. Wang, D. Apelian, D.. Lados, Fatigue behavior of A356-T6 aluminum cast alloys. Part I. Effect of casting defects, *J. Light Met.* 1 (2001) 73–84. doi:10.1016/S1471-5317(00)00008-0.
- [23] J.B. Jordon, M.F. Horstemeyer, N. Yang, J.F. Major, K.A. Gall, J. Fan, et al., Microstructural Inclusion Influence on Fatigue of a Cast A356 Aluminum Alloy, *Metall. Mater. Trans. A.* 41 (2010) 356–363. doi:10.1007/s11661-009-0088-7.
- [24] M. Ulbin, M. Borovinšek, Y. Higa, K. Shimojima, M. Vesenjaj, Z. Ren, Internal structure characterization of AlSi7 and AlSi10 advanced pore morphology (APM) foam elements, *Mater. Lett.* 136 (2014) 416–419. doi:10.1016/j.matlet.2014.08.056.
- [25] S. Terzi, J. a. Taylor, Y.H. Cho, L. Salvo, M. Suéry, E. Boller, et al., In situ study of nucleation and growth of the irregular  $\alpha$ -Al/ $\beta$ -Al<sub>5</sub>FeSi eutectic by 3-D synchrotron X-ray microtomography, *Acta Mater.* 58 (2010) 5370–5380. doi:10.1016/j.actamat.2010.06.012.
- [26] A. Chaijaruwanich, P.D. Lee, R.J. Dashwood, Y.M. Youssef, H. Nagaumi, Evolution of pore morphology and distribution during the homogenization of direct chill cast Al-Mg alloys, *Acta Mater.* 55 (2007) 285–293. doi:10.1016/j.actamat.2006.08.023.
- [27] R.S. Stephenson, M.R. Boyett, G. Hart, T. Nikolaidou, X. Cai, A.F. Corno, et al., Contrast Enhanced Micro-Computed Tomography Resolves the 3-Dimensional

- Morphology of the Cardiac Conduction System in Mammalian Hearts, *PLoS One*. 7 (2012) e35299. doi:10.1371/journal.pone.0035299.
- [28] J.R. Kyle, R.A. Ketcham, Application of high resolution X-ray computed tomography to mineral deposit origin, evaluation, and processing, *Ore Geol. Rev.* 65 (2015) 821–839. doi:10.1016/j.oregeorev.2014.09.034.
- [29] J. Dewanckele, T. De Kock, G. Fronteau, H. Derluyn, P. Vontobel, M. Dierick, et al., Neutron radiography and X-ray computed tomography for quantifying weathering and water uptake processes inside porous limestone used as building material, *Mater. Charact.* 88 (2014) 86–99. doi:10.1016/j.matchar.2013.12.007.
- [30] P. Li, P.D. Lee, T.C. Lindley, D.M. Maijer, G.R. Davis, J.C. Elliott, X-ray Microtomographic Characterisation of Porosity and its Influence on Fatigue Crack Growth, *Adv. Eng. Mater.* 8 (2006) 476–479. doi:10.1002/adem.200600051.
- [31] O. Lashkari, L. Yao, S. Cockcroft, D. Maijer, X-Ray Microtomographic Characterization of Porosity in Aluminum Alloy A356, *Metall. Mater. Trans. A*. 40 (2009) 991–999. doi:10.1007/s11661-008-9778-9.
- [32] N. Vanderesse, É. Maire, A. Chabod, J.-Y. Buffière, Microtomographic study and finite element analysis of the porosity harmfulness in a cast aluminium alloy, *Int. J. Fatigue*. 33 (2011) 1514–1525. doi:10.1016/j.ijfatigue.2011.06.010.
- [33] G. Nicoletto, R. Konečná, S. Fintova, Characterization of microshrinkage casting defects of Al–Si alloys by X-ray computed tomography and metallography, *Int. J. Fatigue*. 41 (2012) 39–46. doi:10.1016/j.ijfatigue.2012.01.006.
- [34] Y. Tijani, A. Heinrietz, W. Stets, P. Voigt, Detection and Influence of Shrinkage Pores and Nonmetallic Inclusions on Fatigue Life of Cast Aluminum Alloys, *Metall. Mater.*

- Trans. A. 44 (2013) 5408–5415. doi:10.1007/s11661-013-1773-0.
- [35] M. Sikandar, H. Khiyal, A. Khan, A. Bibi, Modified Watershed Algorithm for Segmentation of 2D Images, 6 (2009).
- [36] M. De Giovanni, J.M. Warnett, M.A. Williams, N. Haribabu, P. Srirangam, X-ray tomography investigation of intensive sheared Al–SiC metal matrix composites, Mater. Charact. 110 (2015) 258–263. doi:10.1016/j.matchar.2015.11.003.
- [37] J.R. Denton, J.A. Spittle, Solidification and susceptibility to hydrogen absorption of Al–Si alloys containing strontium, Mater. Sci. Technol. 1 (1985) 305–311. doi:10.1179/mst.1985.1.4.305.
- [38] C. Chuang, D. Singh, P. Kenesei, J. Almer, J. Hryn, R. Huff, 3D quantitative analysis of graphite morphology in high strength cast iron by high-energy X-ray tomography, Scr. Mater. 106 (2015) 5–8. doi:10.1016/j.scriptamat.2015.03.017.
- [39] R. Fuoco, E.R. Correa, M. de A. Bastos, Microporosity morphology in A356 aluminum alloy in unmodified and modified condition, AFS Trans. 109 (2001) 659–677.
- [40] S.M. Miresmaeili, J. Campbell, S.G. Shabestari, S.M.A. Boutorabi, Precipitation of Sr-rich intermetallic particles and their influence on pore formation in Sr-modified A356 alloy, Metall. Mater. Trans. A. 36 (2005) 2341–2349. doi:10.1007/s11661-005-0106-3.
- [41] G.K. Sigworth, The Modification of Al-Si Casting Alloys: Important Practical and Theoretical Aspects, Int. J. Met. 2 (2008) 19–40. doi:10.1007/BF03355425.
- [42] Oxford Instruments, TruMap: Real time - real results, (2011).
- [43] E. Sato, N. Kono, I. Sato, H. Watanabe, Study on the phase diagram of Al-Si-Sr ternary alloy system, J. Japan Inst. Light Met. 35 (1985) 71–78.

doi:10.2464/jilm.35.71.

- [44] A.M. Samuel, H.W. Doty, S. Valtierra, F.H. Samuel, Influence of Oxides on Porosity Formation in Sr-Treated Alloys, *Int. J. Met.* (2016) 1–14. doi:10.1007/s40962-016-0118-3.
- [45] M. Felberbaum, E. Landry-Désy, L. Weber, M. Rappaz, Effective hydrogen diffusion coefficient for solidifying aluminium alloys, *Acta Mater.* 59 (2011) 2302–2308. doi:10.1016/j.actamat.2010.12.022.
- [46] J. Campbell, *Castings.*, Butterworth-Heinemann, 2003.

### **3D microstructural studies on porosity and intermetallics formation in strontium modified Al-Si alloys**

**Highlights:**

- X-ray tomography was used to study porosity and intermetallics in Sr modified Al-Si alloys.
- Addition of Sr significantly increased porosity in Al-Si alloys.
- Fine and spherical pores were observed in unmodified alloys compared to modified alloys.
- It is hypothesised that  $\text{Al}_2\text{Si}_2\text{Sr}$  act as sites for porosity nucleation modified Al-Si alloys.